ACS PHYSICAL CHEMISTRY Au
AN OPEN ACCESS JOURNAL OF THE AMERICAN CHEMICAL SOCIETY

pubs.acs.org/physchemau Article

Short-Range Cooperative Slow-down of Water Solvation Dynamics Around SO_4^{2-}–Mg^{2+} Ion Pairs

Achintya Kundu, Shavkat I. Mamatkulov, Florian N. Brünig, Douwe Jan Bonthuis, Roland R. Netz, Thomas Elsaesser, and Benjamin P. Fingerhut*

Cite This: *ACS Phys. Chem Au* 2022, 2, 506–514 Read Online

ACCESS | Metrics & More | Article Recommendations | Supporting Information

ABSTRACT: The presence of ions affects the structure and dynamics of water on a multitude of length and time scales. In this context, pairs of Mg^{2+} and SO_4^{2-} ions in water constitute a prototypical system for which conflicting pictures of hydration geometries and dynamics have been reported. Key issues are the molecular pair and solvation shell geometries, the spatial range of electric interactions, and their impact on solvation dynamics. Here, we introduce asymmetric SO_4^{2-} stretching vibrations as new and most specific local probes of solvation dynamics that allow to access ion hydration dynamics at the dilute concentration (0.2 M) of a native electrolyte environment. Highly sensitive heterodyne 2D-IR spectroscopy in the fingerprint region of the SO_4^{2-} ions around 1100 cm^{-1} reveals a specific slow-down of solvation dynamics for hydrated $MgSO_4$ and for Na_2SO_4 in the presence of Mg^{2+} ions, which manifests as a retardation of spectral diffusion compared to aqueous Na_2SO_4 solutions in the absence of Mg^{2+} ions. Extensive molecular dynamics and density functional theory QM/MM simulations provide a microscopic view of the observed ultrafast dephasing and hydration dynamics. They suggest a molecular picture where the slow-down of hydration dynamics arises from the structural peculiarities of solvent-shared SO_4^{2-}–Mg^{2+} ion pairs.

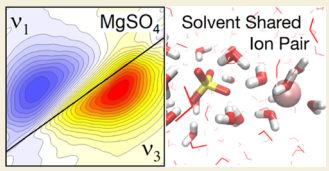

KEYWORDS: *sulfate ions, 2D-IR spectroscopy, molecular dynamics, QM/MM simulations, hydration dynamics, cooperativity*

INTRODUCTION

Interactions of molecules with their environment have a direct impact on their structure and on chemical reactions in the condensed phase. Liquid water, the native medium of biochemical and cellular processes, consists of a complex network of polar molecules and responds to the presence of a solute, both by modification of its local hydrogen-bond structure as well as by modifying the long-range electric force by dielectric screening. Such properties are particularly relevant for accommodating charged species, that is, electrons, protons, and/or molecular ions. The inherent many-body character of the interactions, together with thermally activated ultrafast fluctuations of the water structure, makes studies of the solvation of charged species in water a challenge for both theory and experiment.

Ions in water are embedded in local hydration shells with a structure and dynamics different from the bulk of the liquid. In bulk water, the ultrafast thermal motions of H_2O molecules induce picosecond breaking and formation of hydrogen bonds. Insertion of ions generates local water shells with a different molecular arrangement, hydrogen bond strength, and dynamics.[1,2] In particular, the electrostatic energy is minimized by reorienting the polar water molecules in the first and, to lesser extent, next few solvation shells around the ion site, thus introducing steric constraints and affecting the hydrogen bond structure.

A broad range of experimental methods of structure research and spectroscopy have been applied to unravel equilibrium geometries, dielectric properties, and nonequilibrium elementary excitations of hydrated ions and their impact on water dynamics.[3−14] Regarding the latter, both retarding and accelerating mechanisms have been introduced, including concepts of cooperativity between cations and anions in their impact on the solvent. A large body of molecular dynamics (MD) simulations based on empirical force fields and ab initio simulations has addressed the underlying molecular interactions and provided insight into dynamic hydration geometries.[15−24] Different, in most cases very high ion concentrations in the experiments have led to partly conflicting results, while the complex many-body character of ion solvation in a polarizable liquid represents a major challenge for theoretical and simulation work.

Hydrated sulfate ions are prototypical in this context, given their broad abundance in minerals and their relevance in physiology and biochemistry, for example, of heparin-protein interactions.[25,26] A prominent example is the solvation structures of the SO_4^{2-} ion and (counter)ions such as NH_4^+, Na^+, Ca^{2+}, or Mg^{2+} which have frequently been categorized as spatially uncorrelated free ion pairs (FIP), ion pairs with

Received: August 1, 2022
Revised: September 15, 2022
Accepted: September 15, 2022
Published: October 8, 2022

https://doi.org/10.1021/acsphyschemau.2c00034
ACS Phys. Chem Au 2022, 2, 506–514

separate first water layers around a SO_4^{2-} and a cation in the neighborhood (solvent separated ion pairs, SSIP), ion pairs sharing water molecules in their first solvent shell (solvent shared ion pairs, SIP), and directly interacting contact ion pairs (CIP).[27,28] The relative abundance of the different species and, in particular, the occurrence of CIP has remained highly controversial. For $MgSO_4$, early results from dielectric relaxation and Raman spectroscopy have been interpreted in terms of a simultaneous presence of all species.[8,29] A component of the dielectric spectrum around 10 GHz, changes in the shape of the SO_4^{2-} Raman band at 980 cm^{-1} (ν_1 mode) and a Raman band around 350 cm^{-1} [ν_1 mode of $Mg(OH_2)_6^{2+}$] have been attributed to CIP formation. This view has been challenged by other Raman[30] and THz[11] measurements and, in particular, the comparison of experimental dielectric spectra with those calculated from MD simulations of $MgSO_4$ and Na_2SO_4 in water.[10] A slowing down of the orientational dynamics of water molecules in hydration shells with a cooperative impact of SO_4^{2-} and Mg^{2+} ions has been inferred from polarization-resolved femtosecond pump−probe studies of the water OH stretching vibration in highly concentrated ionic solutions together with THz dielectric relaxation spectroscopy.[12]

The work reported in refs 8, 10−12 and 29 has been performed at ion concentrations of up to several moles/liter (M). Under such conditions, ions are found at an average distance of less than 1 nm and can only accommodate a few water molecules in between.[1] Thus, the space available for water molecules in an undistorted bulk arrangement is substantially diminished and ion−ion interactions as well as the overlap of ion hydration shells become relevant. From a conceptual point of view, SO_4^{2-} vibrations probe local interactions at solvation sites, whereas the water OH stretching response is spatially unspecific and averaged over all water geometries in the ionic solution.

Understanding sulfate hydration at the molecular level requires experimental probes of local dynamics and in-depth theoretical analysis of interactions and MD. Here, we introduce the infrared-active asymmetric stretching vibration of the SO_4^{2-} ion (ν_3 mode) as a local probe of solvation sites and interactions between the ions and their surrounding. Nonlinear two-dimensional infrared (2D-IR) spectroscopy is applied to identify the character and time scale of structural fluctuations and determine their impact on the vibrational line shapes at a moderate 0.2 M concentration of SO_4^{2-} ions in water. To get specific insight into the interactions between SO_4^{2-} and cations in water, $MgSO_4$ and Na_2SO_4 are studied in direct comparison, including samples of Na_2SO_4 with additional Mg^{2+} ions present. In the Na_2SO_4 solution, librational fluctuations of the water shell result in spectral diffusion on a sub-100 fs time scale, followed by slower kinetics. Spectral diffusion is slowed down significantly in the presence of Mg^{2+} ions, both for $MgSO_4$ and Na_2SO_4 with excess Mg^{2+} ions added. This behavior demonstrates a direct impact of Mg^{2+} ions on the water shell of a nearby SO_4^{2-} ion.

The experimental results are complemented by MD simulations and quantum mechanical/molecular mechanical (QM/MM) simulations, which give a quantitative understanding of the vibrational line shape of SO_4^{2-} stretching vibrations, the observed ultrafast dephasing and reorientational water dynamics, as well as the spatial range of water molecules and ions impacting the fingerprint vibrational probe of the SO_4^{2-} tetrahedron. Our results suggest that the slow-down of the water reorientational dynamics observed for $MgSO_4$ arises from water molecules structurally associated with Mg^{2+}−SO_4^{2-} SIP, while there is no evidence for CIP geometries. The two ions of the SIP species induce cooperativity of hydration dynamics in the first two solvation shells already at dilute ion concentrations.

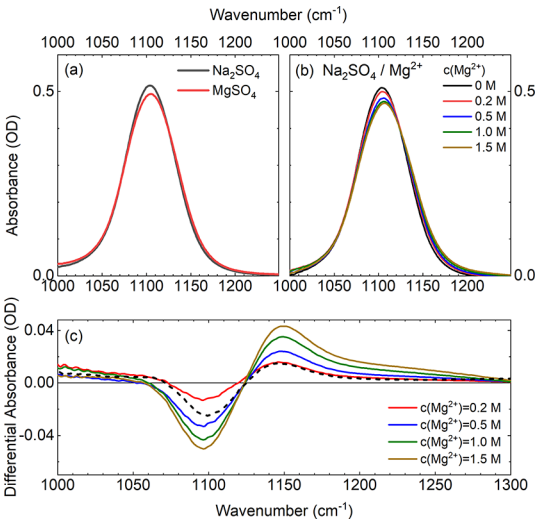

Figure 1. (a) Experimental linear absorption spectra of Na_2SO_4 (black) and $MgSO_4$ (red) in the frequency range of the asymmetric SO_4^{2-} stretching vibration (ν_3 mode, concentrations 0.2 M in water). (b) Linear absorption spectra of Na_2SO_4 (concentration 0.2 M, sample thickness 25 μm) for various added concentrations of $MgCl_2$. (c) Differential linear absorption spectra of Na_2SO_4 and Na_2SO_4 with added $MgCl_2$ as indicated (Na_2SO_4 concentration 0.2 M). The dashed line represents the difference of the $MgSO_4$ and Na_2SO_4 bands shown in panel (a).

RESULTS

Figure 1a shows the linear absorption spectra of Na_2SO_4 and $MgSO_4$ dissolved in water in the frequency range of the asymmetric SO_4^{2-} stretching vibration (ν_3 mode) for an ion concentration of 0.2 M after subtraction of the water background (see the Supporting Information). The isolated sulfate ion SO_4^{2-} has tetrahedral symmetry T_d with three degenerate asymmetric stretching modes and the sulfur atom found in an ideal tetrahedral environment of oxygen atoms. Hydration breaks this molecular symmetry and lifts the degeneracy,[31−33] giving rise to a broad unstructured line shape. The two spectra display a different maximum absorption strength and slightly different line shapes, as is evident from the difference spectrum $\Delta A = A(MgSO_4) - A(Na_2SO_4)$ shown as a dashed line in Figure 1c (absorbance $A = -\log(T)$; sample transmission T). The presence of Mg^{2+} ions causes a decrease of maximum absorption and an absorption shoulder around 1150 cm^{-1}.

The linear absorption spectra of Na_2SO_4 exhibit weak but systematic changes of line shape upon addition of Mg^{2+} ions, as presented in Figure 1b for Mg^{2+} concentrations between 0.2 and 1.5 M (Na_2SO_4 concentration 0.2 M). One observes a decrease in amplitude by about 10% at the maximum of the band (1100 cm^{-1}) and an increase in absorption around 1150 cm^{-1}, as manifested in the difference spectra of Figure 1c and very similar to the differential spectrum of $MgSO_4$ and Na_2SO_4 (dashed line). Such changes are confined to the initial line shape. This behavior is different from Mg^{2+} addition to

https://doi.org/10.1021/acsphyschemau.2c00034
ACS Phys. Chem Au 2022, 2, 506−514

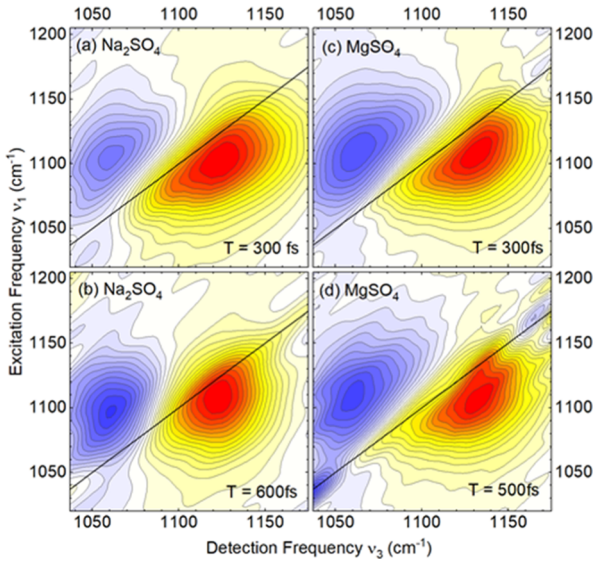

Figure 2. 2D-IR spectra of Na_2SO_4 and $MgSO_4$ for waiting times (a,c) T = 300 fs and (b,d) T = 600 and 500 fs (ion concentrations 0.2 M). Absorptive 2D signals are shown as a function of excitation frequency ν_1 and detection frequency ν_3. Contributions arising from GSB/SE on the ν = 0 → 1 transition are shown with yellow-red contours, and ν = 1 → 2 excited-state absorption contributions are shown in blue. Signal amplitudes are normalized to the maximum GSB/SE signal in each spectrum with a 5% signal change between neighboring contour lines.

phosphate groups in aqueous environment,[34,35] where a new blue-shifted absorption band due to CIP formation with the PO_2^- subgroup arises. The population decay time of the ν_3 mode was measured in femtosecond pump−probe experiments discussed in the Supporting Information. For Na_2SO_4, one observes a decay of the ν = 1 state with a time constant of 290 ± 20 fs.

In Figure 2, 2D-IR spectra of 0.2 M aqueous solutions of Na_2SO_4 (panels a,b) and $MgSO_4$ (panels c,d) are presented for different waiting (population) times T. The absorptive 2D signal (cf. Supporting Information) is plotted as a function of the excitation frequency ν_1 (ordinate) and detection frequency ν_3 (abscissa) and shows contributions arising from ground-state bleaching (GSB) and stimulated emission (SE) on the ν = 0 → 1 transition (yellow-red contours) and contributions arising from excited-state absorption on the ν = 1 → 2 transition (blue contours). At the early waiting time T = 300 fs (Figure 2a,c), the 2D-IR spectra of both samples are characterized by line shapes of the GSB/SE signal stretched along the frequency diagonal $\nu_1 = \nu_3$, reflecting a substantial inhomogeneous broadening due to a distribution of local SO_4^{2-} environments in the liquid.

The 2D-IR spectrum of Na_2SO_4 recorded at T = 600 fs displays a more circular and upright shape of the GSB/SE signal peak compared to the T = 300 fs spectrum. This reshaping is a manifestation of spectral diffusion which is induced by fluctuating forces from the aqueous environment and randomizes the initial distribution of transition frequencies in the ensemble. The change in line shape results in a spectral narrowing of cuts of the 2D-IR spectra along the $\nu_1 = \nu_3$ direction (Figure 3c).

The 2D-IR spectra of $MgSO_4$ (Figure 2c,d) show a minor reshaping with increasing waiting time T, essentially retaining an elliptic shape of the GSB/SE peak. This fact is also evident

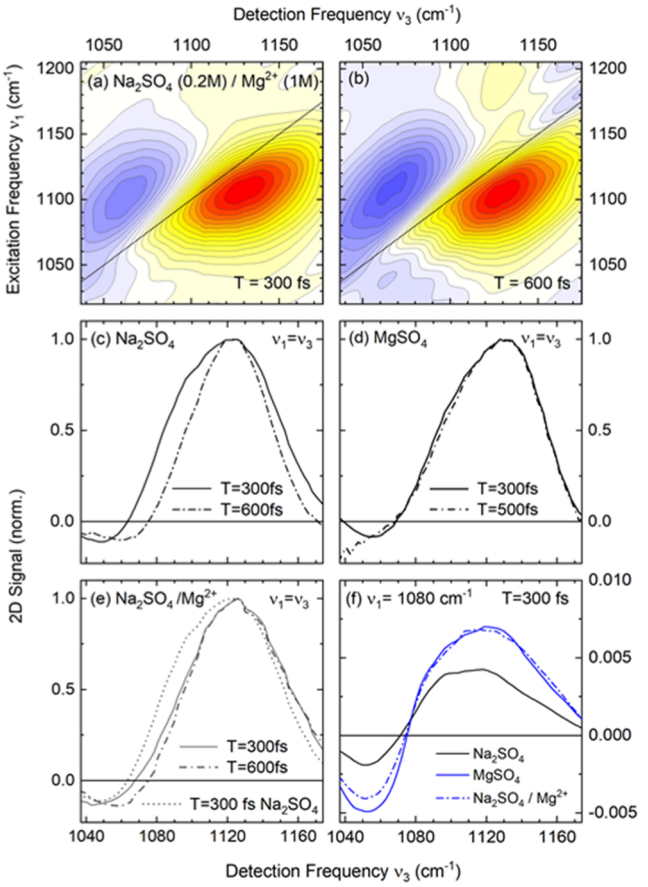

Figure 3. 2D-IR spectra of Na_2SO_4/Mg^{2+} for waiting times of (a) T = 300 fs and (b) T = 600 fs (Na_2SO_4 concentration 0.2 M, Mg^{2+} concentration 1.0 M). (c,d) Frequency cuts of 2D-IR spectra of (c) Na_2SO_4, (d) $MgSO_4$, and (e) Na_2SO_4/Mg^{2+} along a diagonal line parallel to $\nu_1 = \nu_3$ which crosses the maximum of the respective ν = 0 → 1 peak. The dotted line in panel (e) shows the T = 300 fs cut for Na_2SO_4 as a reference. (f) Horizontal cuts of 2D-IR spectra along the detection frequency ν_3 at an excitation frequency ν_1 = 1080 cm^{-1} (waiting time T = 300 fs).

from the nearly identical diagonal cuts for T = 300 and 500 fs (Figure 3d). The very limited change in 2D line shape directly points to a slowing down of spectral diffusion compared to the Na_2SO_4 case and, thus, a modification of the underlying fluctuating forces from the environment in the presence of Mg^{2+} ions.

To explore the impact of Mg^{2+} ions on spectral diffusion more closely, 2D-IR spectra of Na_2SO_4 (c = 0.2 M) with additional Mg^{2+} ions of 1 M concentration were recorded (Figure 3a,b). Most interestingly, the presence of Mg^{2+} ions suppresses the fast reshaping observed in the 2D-IR spectra of the Na_2SO_4 solution (Figure 2a,b). Instead, the 2D-IR spectra for T = 300 and 600 fs and the related diagonal cuts in Figure 3e have a similar shape, exhibiting a persistence of the pronounced inhomogeneous broadening as in the $MgSO_4$ sample.

Cuts of the 2D-IR spectra along the detection frequency ν_3 of the three samples, Na_2SO_4, $MgSO_4$, and Na_2SO_4/Mg^{2+}, reveal a substantial broadening and plateau-like line shape for low excitation frequencies ν_1 = 1080−1120 cm^{-1} compared to excitation frequencies in the range ν_1 = 1130−1150 cm^{-1} (Figure 3f). Such anomalous frequency dependence introduces a slightly trigonal line shape of the 2D-IR spectra in Figures 2

https://doi.org/10.1021/acsphyschemau.2c00034
ACS Phys. Chem Au 2022, 2, 506−514

and 3a,b that points to a cross peak at (ν_1,ν_3) = (1080,1120) cm^{-1} within the 2D envelope and is assigned to a dynamic exchange of subcomponents of the asymmetric SO_4^{2-} stretching vibration.

The 2D-IR line shapes were analyzed by density matrix simulations of the third-order vibrational response[36,37] with a frequency fluctuation correlation function (FFCF) approximated by a sum of Kubo terms. Results of this treatment are presented in the Supporting Information and discussed below.

Atomistic MD and density functional theory QM/MM instantaneous normal mode simulations were employed to obtain microscopic insight into the structure and fluctuation dynamics of sulfate hydration shells, which are made up of water molecules and Na^+ or Mg^{2+} ions. MD simulations employ a SO_4^{2-} force field which has been adapted to reproduce the solvation free energies of single ions and activity coefficients of concentrated solutions (cf. ref 10 and Supporting Information).

The solvation shell of the SO_4^{2-} ion is made up of on average 11.5 water molecules in the first hydration layer (Figure 4a). Each of the four oxygen atoms is coordinated by about three water molecules in a tetrahedral environment. In MD simulations with SO_4^{2-} and Mg^{2+} ions, we find an equilibrium of SIP (Figure 4d), SSIP (Figure 4e), and FIP species,[12] characterized by S···Mg^{2+} distances of ≈0.55 nm, 0.7 nm, and >0.8 nm, respectively (Figure 4b). The double peak found in the radial distribution of S···Mg^{2+} distances of SIP around ≈0.55 nm arise from two possible coordination geometries of bridging water molecules between the Mg^{2+} and SO_4^{2-} ions: either a single water molecule is part of the solvation shell of the Mg^{2+} and the SO_4^{2-} ion or two water molecules bridge the Mg^{2+} and SO_4^{2-} ions in a bidentate coordination (Figure 4d). Each solvation structure is observed with similar probability and interconverts with a mean lifetime of about 10 ps. There is no formation of Mg^{2+}/SO_4^{2-} CIP over the full length of the MD trajectories of 1 μs.

In MD simulations of Na_2SO_4, CIP are in equilibrium with SIP, SSIP, and FIP species [S···Na^+ distances ≈0.35, 0.6, 0.75 and >0.85 nm, Figure 4c]. The weak shoulder in the radial distribution of S···Na^+ distances around 0.35 nm arises from the coordination of the SO_4^{2-} ion by Na^+ ions in the bisector of the O═S═O group (bidentate oxygen coordination). Nevertheless, coordination is observed predominantly via single oxygen atoms of the O═S═O group, characterized by a mean S═O.... Na^+ angle of about 124° being indicative of the replacement of a water molecule in the first solvation shell of the SO_4^{2-} ion by a Na^+ ion. Thus, the predominantly realized CIP coordination geometries resemble the ion pair structures of Na^+ ions with the phosphate groups.[38]

Fluctuation amplitudes of the electric field in the solvent and the underlying dynamics of the hydration shell are imprinted on the line shapes of the linear infrared absorption and nonlinear 2D-IR spectra of the asymmetric SO_4^{2-} stretching mode. A key quantity is the electric field acting on the molecular coordinates of the SO_4^{2-} ion. Here, we consider the electric field projected on the bisector of a SO_2 subgroup and averaged over the six possible permutations of such units in the ion. To characterize the electric field dynamics, we derived the time-dependent field autocorrelation functions $C(t)$ from the MD simulations. In Figure 5, the results are summarized for Na_2SO_4 (green line) and $MgSO_4$ (orange line), together with the components of the $MgSO_4$ function originating from SIP (blue line) and FIP/SSIP (red line).

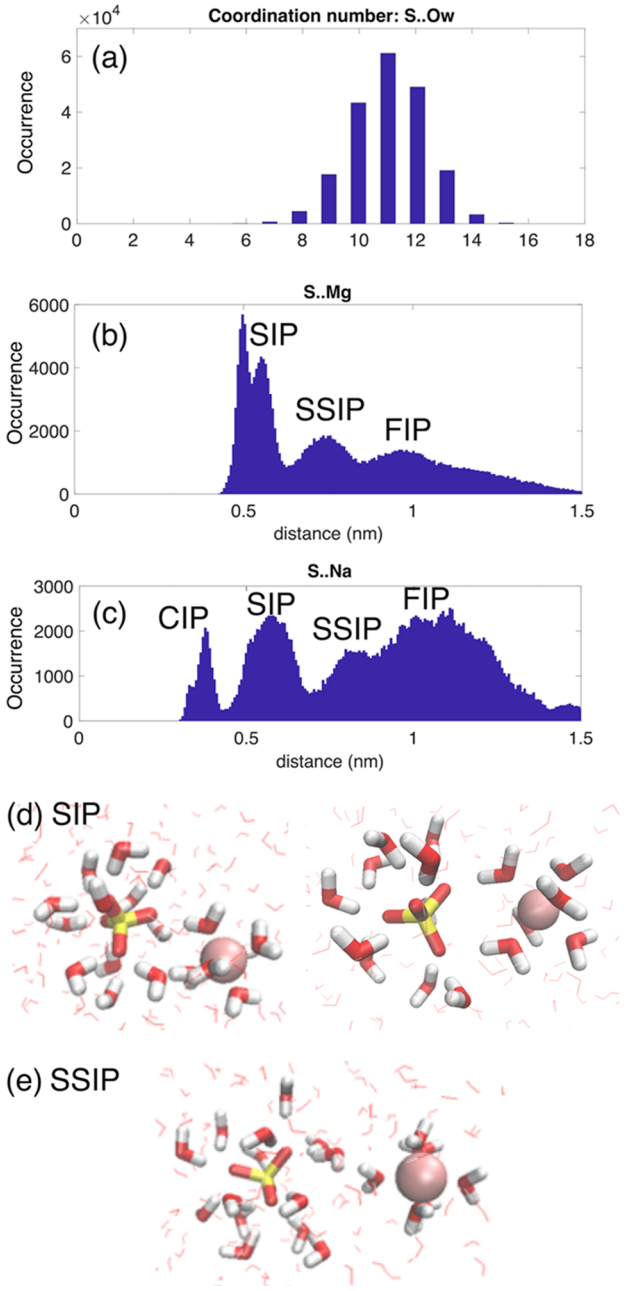

Figure 4. (a) Coordination number of SO_4^{2-} ions by water molecules derived from MD simulations. (b) Radial distribution of sulfur-magnesium (S···Mg^{2+}) distances. (c) Radial distribution of sulfur-sodium (S···Na^+) distances. CIP: contact ion pairs, SIP: solvent shared ion pairs, SSIP: solvent separated ion pairs, FIP: free ion pairs; exemplary molecular SIP bridged by a single molecule (left) or two water molecules (right) and SSIP structures of Mg^{2+} and SO_4^{2-} ions are depicted in panels (d) and (e), respectively. MD simulations were performed with a cubic box (L = 20 Å) of 290 SPC/E water molecules at the respective experimental concentrations of $MgSO_4$ and Na_2SO_4 of about 0.2 M (see the Supporting Information for details).

The different correlation functions consist of an initial femtosecond decay which mainly reflects the librational dynamics of water molecules and a slower decay extending well into the picosecond time range. This slower component is due to rotational motions of water molecules and hydrogen bond breaking and reformation. The correlation functions $C(t)$

https://doi.org/10.1021/acsphyschemau.2c00034
ACS Phys. Chem Au 2022, 2, 506−514

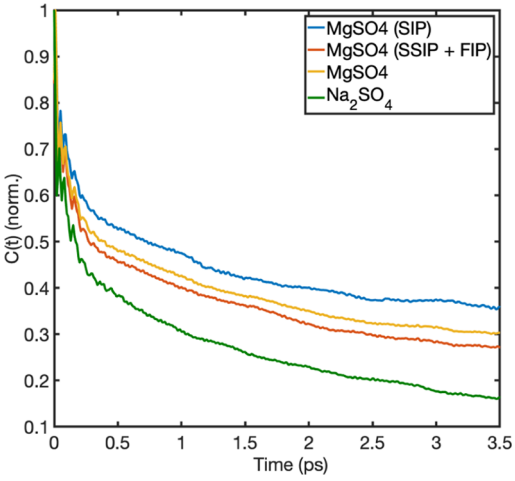

Figure 5. Normalized electric field autocorrelation functions $C(t)$ derived from MD simulations for Na_2SO_4 (green line), $MgSO_4$ (orange line), and components of the $MgSO_4$ correlation function originating from SIP (blue line) and FIP/SSIP (red line). Note the pronounced changes in the relative amplitude of the initial femtosecond decay of correlation.

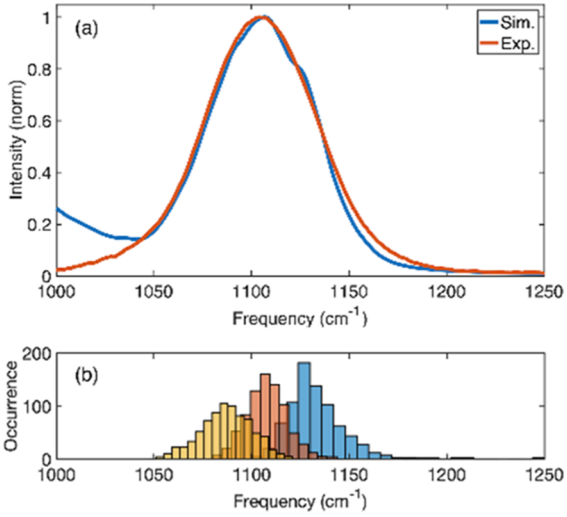

Figure 6. (a) Experimental (red) and simulated (blue, pw6b95-D QM/MM level of theory, see the Supporting Information for details) linear absorption spectra of the asymmetric SO_4^{2-} stretching vibration. (b) Simulated distributions of the subcomponents of the SO_4^{2-} stretching vibration.

of $MgSO_4$ and Na_2SO_4 are best represented by bi- and triexponential fits, respectively, with a fast sub-100 fs time constant and an additional, slightly slower 600 fs time constant for Na_2SO_4 (cf. Supporting Information for details). For Na_2SO_4, the relative amplitude of the fast, sub-picosecond decay is on the order of 0.7, while $MgSO_4$ displays a less prominent fast decay with a relative amplitude of approximately 0.48. This significant decrease in amplitude points to a partial suppression of fast librational water motions in a more rigid solvation environment existing in $MgSO_4$. Decomposition of the overall correlation function into different ionic species of $MgSO_4$ shows a much smaller amplitude of the fast decay for SIP, causing the reduced fast decay component in the overall $C(t)$ of $MgSO_4$. In contrast, the pronounced fast decay components arise for FIP and SSIP geometries (red line), closer to the Na_2SO_4 case (green line). In our simulations of the 2D-IR spectra, we use FFCF with exponential decay components, that is, Kubo terms, mimicking the $C(t)$ functions of Na_2SO_4 and $MgSO_4$.

Density functional theory QM/MM instantaneous normal mode simulations relying on geometries from MD simulations connect the sampled geometries to the spectroscopic observables, allowing to benchmark the sampled structures and thus giving quantitative insight into the hydration dynamics. The theoretical approach allows for quantitative modeling of the linear infrared absorption spectrum, covering the full 1050−1150 cm^{-1} width of the vibrational band (Figure 6a). The large width of the vibrational band arises due to the contributions of three vibrational subcomponents of the asymmetric SO_4^{2-} stretching vibration. Compared to the gas phase, the degeneracy of asymmetric SO_4^{2-} stretching modes is broken in the instantaneous solvent field configuration (Figure 6b). Because of the high sensitivity of the SO_4^{2-} stretching modes to the local environment and the strong coupling to the water librational degrees of freedom, the mode character of the vibrational subcomponents is highly dynamic. On the observation time scale of the 2D-IR experiment set by the vibrational lifetime of some 300 fs, frequency excursions cover the individual subdistributions, and changes of mode character further induce an exchange between the subdistributions, both effects contributing to spectral diffusion.

The performance and accuracy of different density functionals in calculating the linear infrared absorption spectrum were analyzed in a systematic way, and the results are presented in the Supporting Information (Figure S9). Moreover, the size of the QM region was systematically varied in order to demonstrate convergence of the highly accurate simulations of the infrared absorption spectrum of the asymmetric SO_4^{2-} stretching vibration (Figure S10). A faithful agreement of the frequency position in theory and experiment requires to treat the SO_4^{2-} ion and its first solvation shell on the QM level, in turn electrostatically embedded in the remainder of the aqueous environment. A further increase of the QM region to account for water molecules of the second solvation shell does not improve the agreement with the experiment.

DISCUSSION

Our experiments were performed at Na_2SO_4 and $MgSO_4$ concentrations of 0.2 M, much lower than in most studies reported in the literature. The moderate concentration, which corresponds to a ratio of sulfate ions and water molecules of 1:280, allows for uncorrelated ion solvation with several water layers in-between solvation sites. More precisely, the first SO_4^{2-} solvation shell and the first octahedral water shell around a Mg^{2+} ion contains ∼12 and 6 H_2O molecules, respectively. This translates in a concentration of first-shell water of 18 × 0.2 = 3.6 M, which is small compared to the total water concentration of 56 M.

The linear absorption spectra of the asymmetric sulfate stretching vibration (ν_3 mode, Figure 1) exhibit a different line shape for Na_2SO_4 and $MgSO_4$, the latter with a relative enhancement of absorption around 1150 cm^{-1}, within the spectral range covered by the broad absorption bands. A similar enhancement is observed upon gradual addition of Mg^{2+} ions to a Na_2SO_4 solution (Figure 1c). It has been shown that the Raman band of the symmetric SO_4^{2-} vibration (ν_1 mode) of $MgSO_4$ in water develops a high-frequency shoulder

https://doi.org/10.1021/acsphyschemau.2c00034
ACS Phys. Chem Au 2022, 2, 506−514

with increasing ion concentration.[8] Such behavior clearly suggests the impact of a Mg^{2+} ion on the solvation shell of a SO_4^{2-} ion by their close spatial arrangement. However, a direct interpretation of the spectrally broad time-averaged infrared and Raman bands in terms of an ion pairing geometry is speculative and has led to controversy in the existing literature.

The 2D-IR spectra presented in Figures 2 and 3 give direct insight into spectral diffusion and the underlying fluctuation dynamics of SO_4^{2-} solvation shells. The Na_2SO_4 spectra in Figure 2a,b show a pronounced reshaping from an initially elliptic $\nu = 0 \rightarrow 1$ band (yellow-red contours) toward a more round shape. Such changes are a hallmark of spectral diffusion. Our simulation results suggest a highly dynamic mode character of the vibrational subcomponents with frequency excursions within the subdistributions and exchange between subdistributions on the ∼600 fs observation time scale of the experiment. The weak cross peak feature in the 2D-IR line shapes supports the picture of a femtosecond mode exchange with a loss of frequency memory. However, the resolved frequency distributions of Figure 6b show that spectral excursions of the three subcomponents on the ultrafast time scale of the 2D-IR experiment are limited to a frequency interval of approximately 50 cm^{-1}, that is, do not cover the full spectral range of the linear infrared absorption. Otherwise, any frequency resolution within the vibrational lineshape would be diminished, leading to a predominant homogenous broadening mechanism which would not allow to distinguish between Na_2SO_4 and $MgSO_4$ samples.

The fast spectral diffusion and rapid mode exchange are primarily imposed by fast librational water motions in the first and second hydration layers, which translate into fast fluctuations of the local electric field acting on the sulfate ion and cause the prominent femtosecond decay of the electric field autocorrelation function (Figure 5). Because of the short ∼300 fs lifetime of the ν_3 excitations, the 2D-IR spectra mainly reflect such ultrafast fluctuation kinetics, while the slower, mainly reorientational dynamics of the solvent is not visible.

The presence of Mg^{2+} ions changes this picture substantially. The 2D-IR spectra in Figure 2c,d and 3 exhibit a minor reshaping and maintain an elliptic shape throughout the experimental time window limited by the femtosecond population decay of the SO_4^{2-} vibration. The slowing down of spectral diffusion is caused by a reduction of fast structural fluctuations of SO_4^{2-} solvation shells with Mg^{2+} ions nearby. The latter fact is evident from the calculated electric-field autocorrelation functions $C(t)$ in Figure 5 where $MgSO_4$ shows a significantly reduced amplitude of the femtosecond decay in comparison to Na_2SO_4. The analysis of $C(t)$ for the different solvation geometries demonstrates that the reduction of fast fluctuations occurs mainly in SIP arrangements of SO_4^{2-} and Mg^{2+}.

The numerical simulation of the 2D-IR spectra with FFCF mimicking the different components of $C(t)$ for Na_2SO_4 and $MgSO_4$ (cf. Supporting Information) reproduces the main features of the experimental spectra and, thus, provides strong support for this picture. Specifically, the simulations for Na_2SO_4 account reasonably well for the reshaping of the 2D-IR envelope during the initial 600 fs waiting time period, induced by the strong femtosecond components of the FFCF, although the narrowing of the diagonal cut with increasing T is less pronounced in the simulation than in the experiment. In contrast, due to the comparable amplitude of the femtosecond and picosecond correlation decays, the envelopes of the 2D-IR spectra of $MgSO_4$ display negligible changes with waiting time. Because FFCFs are derived from MD simulations that employ a fixed charge force field, the neglect of polarization contributions to spectral diffusion arising from the molecular polarizabilities may be one reason for the remaining discrepancies between simulations and experiment. As an additional caveat, we stress that, as in the case of linear infrared absorption, the 2D-IR spectra represent the average over all ionic arrangements (FIP, SIP, and SSIP) in the sample. As a consequence, any interpretation in terms of ion geometries requires complementary theoretical analysis at molecular length and time scales.

The MD simulation suggests two SIP geometries, one in which a water molecule of the rigid octahedral water shell around Mg^{2+} forms a hydrogen bond with a sulfate oxygen and another one with two bidentate water molecules between the ions (Figure 4d). In both cases, the short water-Mg^{2+} hydrogen bonds restrict fast librational motions and, thus, reduce fast spectral diffusion. The specific slow-down of librations and, on a somewhat longer picosecond time scale, water reorientation are locally restricted to the first solvation shell around the ions, that is, there is no long-range change of water structure. Our results suggest that the nonadditive slow-down of water dynamics for increasing ion concentration[1,12] is associated with the increasing probability of SIP formation, in contrast to the qualitative picture drawn in ref 12.

The radial distributions shown in Figure 4 reveal similar fractions of SIP, SSIP, and FIP geometries, with, however, a stronger relative abundance of SIP in $MgSO_4$ than in Na_2SO_4. Interconversion of the different species by ion and water rearrangements require a reorganization of the hydrogen bond network which occurs on a time scale of 100 ps and beyond and, thus, has a minor influence on the vibrational line shapes.

The MD simulations give a negligible time-averaged number of CIP in $MgSO_4$ and not a single CIP formation event during the 1 μs length of the MD trajectories. While a CIP arrangement of Mg^{2+} and SO_4^{2-} ions is certainly favored by their attractive Coulomb interaction, it would require a hydration shell adapted to the CIP geometry. Here, the rigid octahedral first water shell around Mg^{2+} with short Mg^{2+}—water hydrogen bonds represents a steric boundary condition which may suppress the formation of an appropriate hydration layer around the interacting SO_4^{2-} ion with typically 3 to 4 water molecules per SO unit. In the case of the Na^+/SO_4^{2-}, for which a minor fraction of CIP is predicted by the MD simulation, the more flexible water shell around Na^+ appears to be compatible with CIP formation. It should be noted that CIP formation of Mg^{2+} with sterically less restricting PO_2^- groups has been observed in both model systems and RNA structures.[35,39] A validation of this qualitative discussion requires in-depth structure calculations and experimental work, for example, on clusters, which are beyond the scope of the present study.

In conclusion, our combined experimental and theoretical study reveals a cooperative slow-down of water dynamics around solvent-separated pairs of sulfate and magnesium ions. This slow-down is evident from a significant reduction of spectral diffusion of asymmetric sulfate stretching excitations, which is benchmarked by a direct comparison to the femtosecond spectral diffusion observed in aqueous Na_2SO_4. According to our QM/MM simulations, the slow-down displays a short-range character in space and is due to a restriction of librational water motions in the first and second

https://doi.org/10.1021/acsphyschemau.2c00034
ACS Phys. Chem Au 2022, 2, 506−514

solvation shells around the ions. As a result, fast fluctuations of the electric field from the more rigid first solvation layers are reduced. Contact pairs between sulfate and magnesium ions are absent, while MD simulations predict a minor fraction of sulfate/sodium contact ions in Na_2SO_4 without, however, a clear spectroscopic signature. In contrast to simplistic pictures of structure-making and −breaking ions, which classify the effect of single ions on the water structure and dynamics,[1] our results demonstrate a particular relevance of individual solvation geometries of specific ion pairs for the dynamics of diluted aqueous systems.

MATERIALS AND METHODS

Aqueous solutions of anhydrous $MgSO_4$, Na_2SO_4, and $(NH_4)_2SO_4$ were prepared with a concentration of 0.2 M in ultrapure water. For experiments with additional Mg^{2+} ions, $MgCl_2$ with concentrations from 0.1 to 1.5 M was added to the 0.2 M aqueous solution of Na_2SO_4. A Fourier transform infrared spectrometer was used for recording linear infrared absorption spectra with a spectral resolution of 2 cm^{-1}. The sample thickness was 25 μm. The absorption spectrum of neat water was measured under the same conditions and subtracted from the spectrum of the ionic solutions (cf. Figure 1).

2D-IR spectra were measured in 3-pulse photon-echo experiments with heterodyne detection of the nonlinear signal. Femtosecond infrared pulses with a center frequency of ∼1100 cm^{-1}, a spectral width of ∼190 cm^{-1} (intensity FWHM), and a pulse energy of 5.2 μJ are generated by optical parametric amplification with a 1 kHz repetition rate. Two passively phase-stabilized pulse pairs with wavevectors (k_1, k_2) (mutual delay τ, coherence time) and (k_3, k_{LO}) are generated by reflection from a diffractive optic element. In a box-CARS beam geometry, three pulses are focused into the sample by an off-axis parabolic mirror to generate a photon echo signal. The third-order signal emitted in the phase-matching direction $-k_1 + k_2 + k_3 = k_{Sig}$ is overlapped with a local oscillator pulse (k_{LO}) for spectrally resolved detection by a 64-pixel mercury cadmium telluride detector array (frequency ν_3, spectral resolution 2 cm^{-1}). Signals measured for different coherence times τ are Fourier-transformed along τ to generate the excitation frequency coordinate ν_1. In Figures 2 and 3 and S2−S4 of the Supporting Information, the absorptive 2D-IR signal, which is given by the real part of the sum of the rephasing and nonrephasing signals, is plotted as a function of ν_1 and ν_3. More details on experimental methods are given in the Supporting Information.

MD simulations were performed with the GROMACS 2018 program[40,41] in a cubic box of 290 equilibrated SPC/E water molecules (L = 20 Å) with periodic boundary conditions in all three directions at the experimental concentration of about 0.2 M of $MgSO_4$ and Na_2SO_4, respectively. Following equilibration in the *NVT* and *NPT* ensembles, production run simulations were performed in the *NPT* ensemble (1 bar pressure, T = 300 K) with a time step of 2 fs covering a simulation time of 1 μs. During all simulations, the geometry of SPC/E water molecules was restricted with the SHAKE algorithm. Simulations were performed with the SO_4^{2-} and Mg^{2+} parametrization presented in ref 10. For solutions of Na_2SO_4 and aiming at a balanced description of interaction with the different ions, the recently developed Na^+ ion parameters[42] were employed and, as in the case of $MgSO_4$, a scaling factor λ_σ = 1.65 of modified Lorentz−Berthelot combination rules was used. The employed Na^+/SO_4^{2-} force field parameter combination was verified via the concentration-dependent activity coefficient derivative of the Na_2SO_4 solution (Figure S5).

Time-dependent electric field autocorrelation functions $C(t)$ (Figure 5) consider the electric field amplitude $E(t)$ obtained upon projection of the electric field vector $\vec{E}(t)$ on the bisector of the SO_2 subgroup (cf. Figure S7), followed by averaging over the six possible permutations of such units in the SO_4^{2-} ion. The electric field amplitude $E(t)$ accounts for all partial charges of water molecules and the charges of counter ions Na^+ and Mg^{2+}. Respective field autocorrelation functions $C(t)$ of SIP, SSIP, and FIP hydration species were calculated for consecutive trajectory segments of the individual hydration species with a distance-based criterion for the assignment of hydration species (SIP: S···Mg^{2+} distance $r \leq 0.625$ nm; SSIP: 0.625 nm < $r \leq$ 0.863 nm; FIP: r > 0.863 nm; cf. Figure 4).

QM/MM simulations of vibrational frequencies were performed with NWChem (version 6.3)[43] using a 6-311+G* basis set for the sulfur atom and the 6-31G* basis for all other atoms (O, H, Na, and Mg). Production run simulations (Figure 6) employ the pw6b95 density functional together with Grimme's DFT-D3 dispersion correction[44] (pw6b95-D) and take into account the first solvation shell around the ions on the QM level of theory. The dependence on the employed density functional is explored in Figure S9, and the influence of the QM region on the frequency position and line shape of the asymmetric stretch vibration of the SO_4^{2-} tetrahedron (ν_3 mode) is analyzed in Figure S10. Further details on the theoretical methods are provided in the Supporting Information.

ASSOCIATED CONTENT

Supporting Information

The Supporting Information is available free of charge at https://pubs.acs.org/doi/10.1021/acsphyschemau.2c00034.

Experimental methods, experimental results, simulation of 2D-IR spectra, theoretical methods, and theory results (PDF)

AUTHOR INFORMATION

Corresponding Author

Benjamin P. Fingerhut − *Max-Born-Institut Für Nichtlineare Optik und Kurzzeitspektroskopie, Berlin 12489, Germany;* Present Address: Department Chemie, Ludwig-Maximilians-Universität München, München 81377, Germany; orcid.org/0000-0002-8532-6899; Email: benjamin.fingerhut@cup.lmu.de

Authors

Achintya Kundu − *Max-Born-Institut Für Nichtlineare Optik und Kurzzeitspektroskopie, Berlin 12489, Germany*

Shavkat I. Mamatkulov − *Institute of Material Sciences of Uzbekistan Academy of Sciences, Tashkent 100084, Uzbekistan*

Florian N. Brünig − *Fachbereich Physik, Freie Universität Berlin, Berlin 14195, Germany;* orcid.org/0000-0001-8583-6488

Douwe Jan Bonthuis − *Institute of Theoretical and Computational Physics, Graz University of Technology, Graz 8010, Austria;* orcid.org/0000-0002-1252-7745

Roland R. Netz − *Fachbereich Physik, Freie Universität Berlin, Berlin 14195, Germany;* orcid.org/0000-0003-0147-0162

Thomas Elsaesser − *Max-Born-Institut Für Nichtlineare Optik und Kurzzeitspektroskopie, Berlin 12489, Germany;* orcid.org/0000-0003-3056-6665

Complete contact information is available at: https://pubs.acs.org/10.1021/acsphyschemau.2c00034

Author Contributions

T.E. and B.P.F. initiated, conceived, and supervised the study. A.K. performed the experiments, S.I.M and B.P.F. performed the simulations. All authors contributed to the analysis of the results. B.P.F. and T.E. wrote the manuscript with input from all authors. All authors have given approval to the final version of the manuscript

https://doi.org/10.1021/acsphyschemau.2c00034
ACS Phys. Chem Au 2022, 2, 506−514

Notes

The authors declare no competing financial interest.

■ ACKNOWLEDGMENTS

This research has received funding from the European Research Council (ERC) under the European Union's Horizon 2020 research and innovation program (grant agreements 833365 and 802817) and from the Deutsche Forschungsgemeinschaft (DFG) via the grant IRTG-2662 (434130070).

■ REFERENCES

(1) Marcus, Y. Effect of Ions on the Structure of Water: Structure Making and Breaking. *Chem. Rev.* **2009**, *109*, 1346−1370.
(2) Ohtaki, H.; Radnai, T. Structure and Dynamics of Hydrated Ions. *Chem. Rev.* **1993**, *93*, 1157−1204.
(3) Kim, K. H.; Kim, J.; Lee, J. H.; Ihee, H. Topical Review: Molecular Reaction and Solvation Visualized by Time-Resolved X-Ray Solution Scattering: Structure, Dynamics, and their Solvent Dependence. *Struct. Dyn.* **2014**, *1*, 011301.
(4) Lin, M.-F.; Singh, N.; Liang, S.; Mo, M.; Nunes, J. P. F.; Ledbetter, K.; Yang, J.; Kozina, M.; Weathersby, S.; Shen, X.; Cordones, A. A.; Wolf, T. J. A.; Pemmaraju, C. D.; Ihme, M.; Wang, X. J. Imaging the Short-Lived Hydroxyl-Hydronium Pair in Ionized Liquid Water. *Science* **2021**, *374*, 92−95.
(5) Engel, G.; Hertz, H. G. On the Negative Hydration. A Nuclear Magnetic Relaxation Study. *Ber. Bunsenges. Phys. Chem.* **1968**, *72*, 808−834.
(6) Hertz, H. G.; Zeidler, M. D. Elementarvorgänge in der Hydrathülle von Ionen aus Protonen- und Deuteronenrelaxationszeiten. *Ber. Bunsenges. Phys. Chem.* **1963**, *67*, 774−786.
(7) Barthel, J.; Hetzenauer, H.; Buchner, R. Dielectric relaxation of aqueous electrolyte solutions. I. Solvent Relaxation of 1:2, 2:1, and 2:2 Electrolyte Solutions. *Ber. Bunsenges.Phys. Chem.* **1992**, *96*, 988−997.
(8) Buchner, R.; Chen, T.; Hefter, G. Complexity in "Simple" Electrolyte Solutions: Ion pairing in $MgSO_4$(aq). *J. Phys. Chem. B* **2004**, *108*, 2365−2375.
(9) Wachter, W.; Kunz, W.; Buchner, R.; Hefter, G. Is there an Anionic Hofmeister Effect on Water Dynamics? Dielectric Spectroscopy of Aqueous Solutions of NaBr, NaI, $NaNO_3$, $NaClO_4$, and NaSCN. *J. Phys. Chem. A* **2005**, *109*, 8675−8683.
(10) Mamatkulov, S. I.; Rinne, K. F.; Buchner, R.; Netz, R. R.; Bonthuis, D. J. Water-Separated Ion Pairs Cause the Slow Dielectric Mode of Magnesium Sulfate Solutions. *J. Chem. Phys.* **2018**, *148*, 222812.
(11) Funkner, S.; Niehues, G.; Schmidt, D. A.; Heyden, M.; Schwaab, G.; Callahan, K. M.; Tobias, D. J.; Havenith, M. Watching the Low-Frequency Motions in Aqueous Salt Solutions: The Terahertz Vibrational Signatures of Hydrated Ions. *J. Am. Chem. Soc.* **2012**, *134*, 1030−1035.
(12) Tielrooij, K. J.; Garcia-Araez, N.; Bonn, M.; Bakker, H. J. Cooperativity in Ion Hydration. *Science* **2010**, *328*, 1006−1009.
(13) Park, S.; Odelius, M.; Gaffney, K. J. Ultrafast Dynamics of Hydrogen Bond Exchange in Aqueous Ionic Solutions. *J. Phys. Chem. B* **2009**, *113*, 7825−7835.
(14) Park, S.; Fayer, M. D. Hydrogen Bond Dynamics in Aqueous NaBr Solutions. *Proc. Natl. Acad. Sci. U.S.A.* **2007**, *104*, 16731−16738.
(15) Yadav, S.; Chandra, A. Structural and Dynamical Nature of Hydration Shells of the Carbonate Ion in Water: An Ab Initio Molecular Dynamics Study. *J. Phys. Chem. B* **2018**, *122*, 1495−1504.
(16) Kim, S.; Wang, X. W.; Jang, J.; Eom, K.; Clegg, S. L.; Park, G. S.; Di Tommaso, D. Hydrogen-Bond Structure and Low-Frequency Dynamics of Electrolyte Solutions: Hydration Numbers from ab Initio Water Reorientation Dynamics and Dielectric Relaxation Spectroscopy. *Chemphyschem* **2020**, *21*, 2334−2346.
(17) Tongraar, A.; Rode, B. M. Structural Arrangement and Dynamics of the hydrated Mg^{2+}: An Ab-Initio QM/MM Molecular Dynamics Simulation. *Chem. Phys. Lett.* **2005**, *409*, 304−309.
(18) Wang, X. W.; Toroz, D.; Kim, S.; Clegg, S. L.; Park, G. S.; Di Tommaso, D. Density Functional Theory Based Molecular Dynamics Study of Solution Composition Effects on the Solvation Shell of Metal Ions. *Phys. Chem. Chem. Phys.* **2020**, *22*, 16301−16313.
(19) Vchirawongkwin, V.; Rode, B. M. Solvation Energy and Vibrational Spectrum of Sulfate in Water - An Ab-Initio Quantum Mechanical Simulation. *Chem. Phys. Lett.* **2007**, *443*, 152−157.
(20) Jungwirth, P.; Curtis, J. E.; Tobias, D. J. Polarizability and Aqueous Solvation of the Sulfate Dianion. *Chem. Phys. Lett.* **2003**, *367*, 704−710.
(21) Omta, A. W.; Kropman, M. F.; Woutersen, S.; Bakker, H. J. Negligible Effect of Ions on the Hydrogen-Bond Structure in Liquid Water. *Science* **2003**, *301*, 347−349.
(22) Smith, J. D.; Saykally, R. J.; Geissler, P. L. The Effects of Dissolved Halide Anions on Hydrogen Bonding in Liquid Water. *J. Am. Chem. Soc.* **2007**, *129*, 13847−13856.
(23) Lin, Y. S.; Auer, B. M.; Skinner, J. L. Water Structure, Dynamics, and Vibrational Spectroscopy in Sodium Bromide Solutions. *J. Chem. Phys.* **2009**, *131*, 14451.
(24) Verde, A. V.; Lipowsky, R. Cooperative Slowdown of Water Rotation near Densely Charged Ions is Intense but Short-Ranged. *J. Phys. Chem. B* **2013**, *117*, 10556−10566.
(25) Capila, I.; Linhardt, R. J. Heparin-Protein Interactions. *Angew. Chem., Int. Ed.* **2002**, *41*, 390−412.
(26) Nie, C.; et al. Polysulfates Block SARS-CoV-2 Uptake through Electrostatic Interactions. *Angew. Chem., Int. Ed.* **2021**, *60*, 15870−15878.
(27) Eigen, M.; Tamm, K. Schallabsorption in Elektrolytlösungen als Folge chemischer Relaxation I. Relaxationstheorie der mehrstufigen Dissoziation. *Z. Elektrochem., Ber. Bunsenges. Phys. Chem.* **1962**, *66*, 93−107.
(28) Eigen, M.; Tamm, U. K. Schallabsorption in Elektrolytlösungen als Folge chemischer Relaxation II. Meßergebnisse und Relaxationsmechanismen für 2—2-wertige Elektrolyte. *Z. Elektrochem., Ber. Bunsenges. Phys. Chem.* **1962**, *66*, 107−121.
(29) Rudolph, W. W.; Irmer, G.; Hefter, G. T. Raman Spectroscopic Investigation of Speciation in $MgSO_4$(aq). *Phys. Chem. Chem. Phys.* **2003**, *5*, 5253−5261.
(30) Rull, F.; Balarew, C.; Alvarez, J. L.; Sobron, F.; Rodriguez, A. Raman Spectroscopic Study of Ion Association in Aqueous Magnesium Sulphate Solutions. *J. Raman Spectrosc.* **1994**, *25*, 933−941.
(31) Pye, C. C.; Rudolph, W. W. An Ab-Initio and Raman Investigation of Sulfate Ion Hydration. *J. Phys. Chem. A* **2001**, *105*, 905−912.
(32) Zhou, J.; Santambrogio, G.; Brümmer, M.; Moore, D. T.; Wöste, G.; Meijer, D. M.; Neumark, K. R.; Asmis, K. R. Infrared Spectroscopy of Hydrated Sulfate Dianions. *J. Chem. Phys.* **2006**, *125*, 111102.
(33) Knorke, H.; Li, H. Y.; Warneke, J.; Liu, Z. F.; Asmis, K. R. Cryogenic Ion Trap Vibrational Spectroscopy of the Microhydrated Sulfate Dianions $SO_4^{2-}(H_2O)_{(3-8)}$. *Phys. Chem. Chem. Phys.* **2020**, *22*, 27732−27745.
(34) Schauss, J.; Dahms, F.; Fingerhut, B. P.; Elsaesser, T. Phosphate-Magnesium Ion Interactions in Water Probed by Ultrafast Two-Dimensional Infrared Spectroscopy. *J. Phys. Chem. Lett.* **2019**, *10*, 238−243.
(35) Schauss, J.; Kundu, A.; Fingerhut, B. P.; Elsaesser, T. Contact Ion Pairs of Phosphate Groups in Water: Two-Dimensional Infrared Spectroscopy of Dimethyl Phosphate and ab Initio Simulations. *J. Phys. Chem. Lett.* **2019**, *10*, 6281−6286.
(36) Siebert, T.; Guchhait, B.; Liu, Y. L.; Costard, R.; Elsaesser, T. Anharmonic Backbone Vibrations in Ultrafast Processes at the DNA-Water Interface. *J. Phys. Chem. B* **2015**, *119*, 9670−9677.
(37) Hamm, P.; Zanni, M.*Concepts and Methods of 2D Infrared Spectroscopy*; Cambridge University Press: Cambridge, 2011.

(38) Fingerhut, B. P.; Schauss, J.; Kundu, A.; Elsaesser, T. Aqueous Contact Ion Pairs of Phosphate Groups with Na^{+}, Ca^{2+} and Mg^{2+}-Structural Discrimination by Femtosecond Infrared Spectroscopy and Molecular Dynamics Simulations. *Z. Phys. Chem.* **2020**, *234*, 1453−1474.
(39) Schauss, J.; Kundu, A.; Fingerhut, B. P.; Elsaesser, T. Magnesium Contact Ions Stabilize the Tertiary Structure of Transfer RNA: Electrostatics Mapped by Two-Dimensional Infrared Spectra and Theoretical Simulations. *J. Phys. Chem. B* **2021**, *125*, 740−747.
(40) Berendsen, H. J. C.; van der Spoel, D.; van Drunen, R.; GROMACS, R. A message-passing parallel molecular dynamics implementation. *Comput. Phys. Commun.* **1995**, *91*, 43−56.
(41) Lindahl, E.; Hess, B.; van der Spoel, D. GROMACS 3.0: a package for molecular simulation and trajectory analysis. *J. Mol. Model.* **2001**, *7*, 306−317.
(42) Loche, P.; Steinbrunner, P.; Friedowitz, S.; Netz, R. R.; Bonthuis, J. D. Transferable Ion Force Fields in Water from a Simultaneous Optimization of Ion Solvation and Ion−Ion Interaction. *J. Phys. Chem. B* **2021**, *125*, 8581−8587.
(43) Valiev, M.; Bylaska, E. J.; Govind, N.; Kowalski, K.; Straatsma, T. P.; Van Dam, H. J. J.; Wang, D.; Nieplocha, J.; Apra, E.; Windus, T. L.; de Jong, W. A. NWChem: A Comprehensive and Scalable Open-Source Solution for Large Scale Molecular Simulations. *Comput. Phys. Commun.* **2010**, *181*, 1477−1489.
(44) Grimme, S.; Antony, J.; Ehrlich, S.; Krieg, H. A Consistent and Accurate Ab Initio Parametrization of Density Functional Dispersion Correction (DFT-D) for the 94 Elements H-Pu. *J. Chem. Phys.* **2010**, *132*, 154104.

https://doi.org/10.1021/acsphyschemau.2c00034
ACS Phys. Chem Au 2022, 2, 506−514